Czaja, P.; Szczerba, M.J.; Chulist, R.; Balanda, M.; Przewoznik, J.; Chumlyakov, Y.I.; Schell, N.; Kapusta, Cz.; Maziarz, W.:

Martensitic transition, structure and magnetic anisotropy of martensite in Ni-Mn-Sn single crystal

In: Acta Materialia (2016) Elsevier

DOI: 10.1016/j.actamat.2016.07.059

Martensitic transition, structure and magnetic anisotropy of martensite in Ni-Mn-Sn single crystal

P. Czaja[a,*], M. J. Szczerba[a], R. Chulist[a], M. Bałanda[b], J. Przewoźnik[c], Y. I. Chumlyakov[d], N. Schell[e], Cz. Kapusta[c], W. Maziarz[a]

[a] *Institute of Metallurgy and Materials Science, Polish Academy of Sciences, 25 Reymonta St., 30-059 Kraków, Poland*

[b] *The Henryk Niewodniczanski Istitute of Nuclear Physics, Polish Academy of Sciences, 152 Radzikowskiego St., 31-342 Kraków, Poland*

[c] *AGH University of Science and Technology, Faculty of Physics and Applied Computer Science, Department of Solid State Physics, Al. Mickiewicza 30, 30-059 Kraków, Poland*

[d] *Siberian Physical-Technical Institute, Tomsk 634050, Russia*

[e] *Institute of Materials Research, Helmholtz-Zentrum Geesthacht, Max-Planck-Strasse 1, D-21502 Geesthacht, Germany*

Abstract

The structural and magnetic properties of $Ni_{50}Mn_{37.5}Sn_{12.5}$ single crystal were investigated. The alloy undergoes martensitic transformation at 308 K from the austenite phase to the structurally modulated tetragonal 4M martensite phase with lattice parameters a_{4M} = 6.177 Å, c_{4M} = 5.669 Å. The alloy shows 7.9% pre-strain upon uniaxial compression along the <001> direction, which is near the theoretical 8.2% maximum twinning strain. Magnetization measurements reveal that the magnetic anisotropy of the martensite phase is uniaxial with the easy magnetization axis corresponding to the shortest *c* axis of the tetragonally distorted unit cell, while its *a* axis is the hard magnetization direction. The magnetic anisotropy constant K_u saturates at low temperature around 7×10^4 J/m^3 and then gradually decreases with increasing temperature as the system approaches the Curie temperature of martensite at 215 K.

Key words: Martensitic transformation; Heusler alloys; Magnetic shape memory alloys; Magnetic shape anisotropy; Single crystal.

I. Introduction

Magnetic field induced reverse martensitic transformation (MFIRMT) is a phenomenon resembling the conventional shape memory effect due to heating with the exception that it is triggered by the action of a magnetic field [1]. It may then offer frequency response higher than conventional, which makes it interesting for actuation and sensing applications. MFIRMT is displayed by a special class of magnetic shape memory alloys (MSMA), often referred to as metamagnetic shape memory alloys such as Ni-Mn-(Sn, Sb, In) [1]. The transformation proceeds between the weakly magnetic martensite phase and ferromagnetic austenite [2,3]. The driving force for the transition along some contribution from the magnetocrystalline anisotropy energy (MAE) is predominantly the Zeeman energy ($ZE=\Delta M \cdot H$) arising from the different saturation magnetization between martensite and austenite [4]. Unlike MAE the ZE is less sensitive to the crystal orientation, it can continuously increase with the field and it can be maximized by enhancing the magnetization

* Corresponding author. E-mail address: p.czaja@imim.pl (P. Czaja)

difference between the transforming phases for instance by doping with Co, which is known to increase the Curie temperature of the austenite phase (T_C^A) in ternary Ni-Mn-(In, Sn) based alloys [5,6]. Henceforth the *ZE* difference can yield considerable actuation stress on the order of 100 MPa greatly exceeding that of earlier MSMA such as Ni-Mn-Ga based alloys, which are capable of up to 12% recoverable magnetic field induced strain (MFIS) but at an order of magnitude lower output stress level (~2 MPa) [7,8]. This is associated with a different mechanism of MFIS in the latter, which is based on the twin boundary motion governed by MAE [9,10,11]. Similar to conventional SME an introduction of a pre-strain to the martensite phase is a prerequisite for large MFIS (due to MFIRMT). An almost full recovery of such a 3% deformation has been reported under 7 T in a single crystalline Ni-Co-Mn-In alloy, which aroused some attention [1]. A transformation strain of 5.4% under 125 MPa thermal cycling was reported in the same system [12] and more recently a 3.1% completely recoverable MFIS due to MFIRMT was noted in single crystal of $Ni_{45}Co_5Mn_{36.5}In_{13.5}$ alloy [13,14]. A lower recovery strain amounting to 77% of the initial 1.3% pre-strain was observed in polycrystalline $Ni_{43}Co_7Mn_{39}Sn_{11}$ alloy. Simultaneously this system showed a spontaneous 0.3% length change upon removal of the magnetic field, which indicated a two way shape memory effect not detected previously in single crystalline Ni-Co-Mn-In. This effect was ascribed to the presence of constraint stress at grain boundaries acting as nucleation sites for strained martensite [15]. Despite this initially encouraging results there are still pertaining issues *e*. *g*. the reduction of the critical magnetic field, and shortening of the transformation hysteresis etc., which need to be addressed in order to advance the dawn of practical applications [16,17]. These challenges are also relevant to other functional properties shown by MSMA such as giant magnetoresistance [18], exchange bias [19] and magnetocaloric effect [20], the potential of which could be harnessed in combination with magneto mechanical response of MSMA resulting in effective multiferroic systems [21]. For example lately a large elastocaloric effect (4 K) was found during loading polycrystalline $Ni_{45}Mn_{44}Sn_{11}$ alloy at 291 K with a 1.3% transformation strain [22]. In the early reports it was suggested that Ni-Mn-Sn with modulated orthorhombic (4O) martensite structure should show low twinning stress ($\beta = 90^{\circ}$) yielding considerable twin mobility and therefore a considerable pre-strain critical for MFIS [23]. Up to date this was not, however, verified experimentally largely due to difficulty in obtaining single crystalline Ni-Mn-Sn specimen [24]. In this letter we report on the microstructure, martensitic transformation, pre-strain and magnetic anisotropy of martensite in $Ni_{50}Mn_{37.5}Sn_{12.5}$ single crystalline alloy. This contribution should enhance the fundamental understanding of the unique properties of these systems and henceforth should aid the control of their functionalities in the future.

II. Experimental procedures

$Ni_{50}Mn_{37.5}Sn_{12.5}$ single crystal was grown using the Bridgman method from an ingot prepared in advance by induction melting from high purity Ni, Mn, Sn (99.99%). It was then annealed at 1220 K for 72 h to ensure chemical homogeneity. The composition of the single crystal was $Ni_{49.5\pm1}Mn_{38.4\pm0.8}Sn_{12.2\pm0.2}$ as determined according to X-ray energy dispersive spectroscopy (EDS) analyser fitted to FEI E-SEM XL30 scanning electron microscope (SEM). Subsequently the crystal was oriented using the energy backscattered electron diffraction (EBSD) technique on high resolution field emission FEI Quanta 3D instrument equipped with an EBSD detector and then cut into a 4.16 mm × 2.74 mm × 1.72 mm rectangular prism by spark erosion along the {100} planes of the parent $L2_1$ cubic phase.

Mechanical training was performed on an Instron testing machine at room temperature under a compressive stress of up to 250 MPa and at a strain rate of 10^{-3} s^{-1}. The microstructure was studied using Tecnai G2 (200 kV) transmission electron microscope. Thin foils for TEM examination were prepared by first cutting a slice (circa 0.15 mm thick) from the bulk sample along the {001} type plane referred to the austenite phase with a precision wire saw, mechanically grinding it and finally electro polishing using TenuPol-5 double jet electropolisher and an electrolyte of nitric acid (1/3) and methanol (2/3) at 240 K. Crystal structure and lattice parameters of the martensite phase at room temperature were determined on the bulk single crystal by synchrotron high energy X-ray radiation (87.1 keV, λ=0.14236 Å) at the beamline Petra P07B at Desy (Hamburg, Germany). High energy synchrotron radiation enables measurements in transmission geometry, which significantly improved the variant statistics of this sample. The DC mass magnetic susceptibility (and magnetization) was measured in the temperature range from 2 K up to 380 K and in the magnetic field of 5 mT (and 5 T) using Vibrating Sample Magnetometer (VSM) option of the Quantum Design Physical Property Measurement System (PPMS-9).

III. Experimental results and discussion

At room temperature the specimen shows a self-accommodated (SA) martensite microstructure with pairs of twin variants arranged into variant colonies (Fig. 1) [25]. The martensite structure is further confirmed by TEM. Fig. 2 (a) shows Bright Field (BF) image of two martensite plates separated by a twin boundary. The inset picture presents the corresponding Selected Area Diffraction Pattern (inset) taken from the single martensite variant. Three extra spots in between the main reflections suggest the modulated 4M structure [23]. Fig. 2 (b) displays the diffraction pattern taken from two twinned variants (V1 and V2) with nearly orthogonal modulation direction. The modulation period determined by High Resolution TEM (HREM) appears to be $(3\bar{1})$ according to Zhdanov notation and it is indicated by the step like red and white line (Fig. 2 (c)). The crystal structure and lattice parameters of the martensite phase for the $Ni_{49.5}Mn_{38.4}Sn_{12.2}$ specimen were further confirmed using high energy Synchrotron radiation. Fig. 3 shows the 2D diffraction pattern of martensite. It is explicit that martensite has a modulated structure in accordance with previous TEM analysis (Fig. 2). The crystal structure is determined to be 4-layered tetragonal structure with the following lattice parameters: a_{4M} = 6.177 Å and c_{4M} = 5.669 Å. From this the maximum twining strain given as $\epsilon_0 = (1 - c/a)$ can be deduced as amounting to 8.22%. It should be mentioned that the lattice parameters and the maximum strain for the 4M Ni-Mn-Sn structure is given with respect to the so-called “cubic coordinate system”, which is related to the cubic axes of the parent $L2_1$ austenite.

In order to determine the magnetic ordering temperatures and study the behaviour of the MT the low field (5 mT) zero field cooled (ZFC), field cooled (FC) and field heated (FH) dc mass magnetic susceptibilities χ were measured as a function of temperature $(\chi)T$. Before ZFC the sample was cooled down from 380 K to 2 K at no applied magnetic field, then ZFC measurement was performed at 5 mT with temperature increasing up to 380 K. Subsequently FC and FH measurements were performed at the same field upon decreasing and increasing the temperature, respectively. All the measurements were performed in a step mode with stabilised temperature at each experimental point. The magnetic transformation temperatures corresponding to the Curie temperature of austenite (T_C^A) and martensite (T_C^M) and the

structural transformation temperatures of the forward austenite to martensite ($T_{pA\rightarrow M}$) and reverse transformations ($T_{pM\rightarrow A}$) were taken as the inflection points of the corresponding χ(T) dependences at 5 mT. The characteristic martensite start (M_s), martensite finish (M_f) for the forward MT and the austenite start (A_s) and austenite finish (A_f) temperatures for the reverse MT were determined with the tangential method from the FC and FH thermomagnetic curves measured at 5 mT, 0.5 T, 2 T, 5 T and 9 T. Fig. 4 (a) shows the ZFC, FC and FH χ(T) curves for the SA $Ni_{49.5}Mn_{38.4}Sn_{12.2}$ single crystal under 5 mT and 5 T applied magnetic field. It can be seen from the curves that on cooling the single crystal undergoes martensitic transformation from the paramagnetic austenite phase to a weakly magnetic martensite, which is given away by a magnetization change around 310 K. The forward transformation temperature ($T_{pA\rightarrow M}$) determined from the inflection point of the FC χ(T) curve at 5 mT is equal to 308 K, whereas the Curie transition of austenite is determined at T_C^A = 311 K. On further cooling the martensite phase orders ferromagnetically at the Curie transition of martensite at T_C^M = 215 K. The bifurcation between the ZFC and FC curves may suggest magnetic inhomogeneity or a coexistence of antiferromagnetic-ferromagnetic interfaces, which are frequently encountered in Mn-rich Ni-Mn based alloys [3,19,26]. The reverse transformation ($T_{pM\rightarrow A}$) occurs at 307 K as determined from FH curve. At this point it needs to be remarked that due to the close proximity between the martensitic and magnetic transformation temperatures the temperatures estimation may not be as accurate. A closer look at the magnified χ(T) curve in the 260 – 360 K temperature range (the inset picture) reveals a transformation hysteresis typical for first order transitions. The corresponding onset and finish temperatures for the forward and reverse transformations are determined at 5 mT as follows: M_s= 333 K, M_f = 301 K, A_s = 295 K, A_f = 343 K. The double loop like appearance of the χ(T) curves within the transformation temperature range ($M_f \leq T \leq M_s$) is attributed to the coincidence of the structural and magnetic transformation temperatures, that is austenite undergoes magnetic transition while transforming to or from martensite on the forward and reverse MT, respectively. At higher field this effect subsides. This is illustrated in the inset picture in Fig. 4 (a) and in Fig. 4 (b), which shows M vs. T dependence under the applied magnetic field from 0.5 to 9 T. The characteristic M_s, M_f, A_s, A_f temperatures determined from the respective FC and FH curves at higher magnetic fields are collected in Table 1 along with the values of the transformation hysteresis given as: A_f - M_s or A_s - M_f and transformation interval calculated as: M_s - M_f and A_f - A_s. The hysteresis is around 12 K, which is consistent with the hysteresis values reported for other Ni-Mn-Sn alloys and comparable to $Ni_{55}Mn_{20}Ga_{25}$ single crystalline alloy [22,27,28,29,30,31,32]. The transformation interval is around 20 K. The negligible effect of the magnitude of the magnetic induction field on the characteristic forward and reverse transformation temperatures is illustrated schematically in Fig. 4 (b) and in the inset in that figure. According to Fig. 4 (b) the loops do not show a prominent temperature shift with increasing field. The inset shows the M_s, M_f, A_s, and A_f characteristic temperatures dependence on the magnetic field intensity. Initially with increasing magnetic field from 0.5 to 2 T the M_s increases from 329 to 331 K but this is marginal. At the same time A_s appears to be less sensitive to changes in $\mu_0 \cdot H$. This effect can be traced down to the relative positions between M_s and T_C^A temperatures. It transpires from the above that the onset of the martensitic transformation is located well above the Curie point of austenite and from this reason the magnetic field does not seem to exert much influence on the temperature shift of MT since the driving force, as given by the Clausius-Clapeyron relation ($\Delta T = \left(\frac{\Delta M}{\Delta S}\right)\Delta H$), is not pronounced enough due to negligible magnetization

difference between paramagnetic austenite and weakly magnetic martensite among which the MT takes place. In fact in this instance the M_s temperature appears above A_s (inset Fig. 4 (b)) unlike in the case of other MSMA with well divorced magnetic and structural transformation temperatures [31]. This indicates stronger magnetization in the martensite phase than in austenite within the transformation range as can also be seen from the respective $M(H)$ isotherms shown in Fig. 5. The figure shows the dependence of FC (under 5 T) magnetization, M (given in μ_B per Mn atom) on the applied magnetic field $\mu_0 \cdot H$ for the studied single crystal at the 3-350 K temperature range. The inset picture in Fig. 5 shows the magnetic isotherms measured in the temperature range close to the reverse MT. It is visible from the magnetization hysteresis that the field begins to induce the reverse transformation at circa 310 K. The hysteresis becomes more pronounced at 330 K.

The coexistence of FM and AFM domains in the low temperature martensite phase is verified by confirming the Exchange Bias (EB) effect. EB is manifested by the shift of the magnetic hysteresis loop towards negative field axis when the material is cooled under a positive external magnetic field. In this study the sample was subjected to FC down to 3 K at +5 T and subsequently the loop was measured at this temperature while cycling the magnetic field within ± 9 T range. ZFC measurement after cooling under no applied magnetic field down to 3 K was also performed at 3 K within ± 9 T. The inset picture in Fig. 6 for the sake of clarity shows parts of the $M(H)$ magnetic hysteresis loop determined in the ZFC mode. A characteristic symmetric, double shifted character of the loops is noted from the picture, which is a signature of different magnetic anisotropy phases typical for an EB system. The $M(H)$ loop measured in the FC mode are shown in parts in Fig. 6. The EB (H_E) and coercive (H_C) fields were determined from the loops as $H_E=-(H_1+H_2)/2$ and $H_C=|H_1-H_2|/2$, where H_1 and H_2 are the left and right coercive fields at zero magnetization and are shown in the inset in Fig. 12.

In order to study pre-strain and magnetic anisotropy of the martensite phase the sample was subjected to a training procedure, which allows for translating of the self-accommodated multivariant microstructure into a single variant (SV) state [25]. The training involves a sequence of uniaxial compression tests along the <001> crystallographic directions. The mechanism of this processes is based on the twin variant interactions within a complex twinned microstructure. This phenomena is elaborated in more details elsewhere [25,33,34,35]. Fig. 7 shows the stress – strain curves documenting the mechanical history of the specimen during the training procedure. The inset picture in Fig. 7 presents the schematics of the compression experiment with the load direction (σ) represented by red arrows and V_{1x}, V_{1z}, V_{2y}, V_{2z}, V_{3x} and V_{3y} standing for six possible twin variant configurations of martensite. The first compression marked in Fig. 7 was performed parallel to z axis. It is observed from the curve that following the initial elastic strain range the sample begins to deform plastically by twin boundary migration, which promotes twin variants oriented with their shorter c axis along the compression direction. The onset of this transformation is set at ca. 37 MPa, which indicates the magnitude of yield stress required to initiate this process. As the deformation proceeds the stress gradually decreases, which is combined with mechanical instabilities resulting from activation of different twinning modes. The compression test is terminated at the point where the plastic deformation through twin boundary migration is exhausted and the martensite phase starts to deform elastically. The first compression test was accompanied by a 5.2% decrease in dimension along z direction and a simultaneous 2.4% and 1.5% increase in dimensions along x and y directions. This is schematically illustrated in Fig. 8, which shows

the changes to the x, y and z dimensions measured after each step of the mechanical training: $\frac{x_{i+1}-x_i}{x_i}\times100\%$, $\frac{y_{i+1}-y_i}{y_i}\times100\%$, $\frac{y_{i+1}-y_i}{y_i}\times100\%$ [33]. Such behaviour accompanying the first compression test indicates that the strain is mediated by $V_{1z} \rightarrow V_{1x}$ and $V_{2z} \rightarrow V_{2y}$ reorientation with clear anisotropy along x axis at the expense of y axis, which is reflected in the larger strain along x direction. The second compression along x axis, involved 7.9% decrease along x, an equal expansion along z and marginal (0.4%) expansion in y direction. This is also well visible in Fig. 8 from the distinct change in the positions of x and z corresponding to the change in sample dimensions relative to their previous values along x and z axis, respectively. In this instance the reorientation can take place between $V_{1x} \rightarrow V_{1z}$ and $V_{3x} \rightarrow V_{3y}$ modes, however in view of insignificant strain along the y axis after the second compression primarily V_{1z} variant is expected to be found in the sample. During the third compression test the load was reapplied along z axis yielding 7.4% decrease and equivalent increase along z and x directions, respectively. The length change along the y axis remained at the constant level of 0.4%. The last and fourth compression was performed along the x axis. From these results it can be concluded that after the second compression test the observed strain is associated primarily with interaction between V_{1x} and V_{1z}, which switch into one another upon loading the sample in the respective direction. This implies some pre-existing anisotropy in the sample. After the fourth compression the martensite microstructure should be chiefly based on the V_{1z} variant with the shortest *c* axis along the x direction. This is confirmed by measuring (001) type pole figures prior to the training and afterwards (Fig. 9). It is also noted from Fig. 7 that after the first compression and thereafter the twining stress decreases in each next test due to the change in twinned microstructure, what is often observed in other MSMA [36]. The inset picture in Fig. 8 shows the $\vec{\boldsymbol{a}}$, $\vec{\boldsymbol{b}}$, $\vec{\boldsymbol{c}}$ vectors corresponding to crystal lattice directions after training.

Following the mechanical treatment the magnetic properties were determined for the $Ni_{49.5}Mn_{38.4}Sn_{12.2}$ single crystal in single variant martensite state. Fig. 10 shows the magnetization curves measured after ZFC and FC (5 T) along the [100], [010] and [001] directions at 3 K. The sample was mechanically constrained during the measurement in order to avoid redistribution of martensite variants imposed by the action of magnetic field. It is clear from Fig. 10 that the magnetic anisotropy is uniaxial with magnetization easy axis corresponding to the shortest *c* axis of the tetragonal distortion, while *a* and *b* axes are hard magnetization directions. This is consistent with structural data. The magnetization curves display negligible hysteresis and the curve recorded along the hard direction is linear almost to saturation, which confirms that the magnetization process is governed by rotation of the magnetic moment and it receives insignificant contribution from domain wall motion. The temperature dependence of FC hysteresis loops measured after cooling at 5 T was further studied to investigate the effect of easy axis on EB properties. Fig. 11 shows parts (for clarity, full loops are shown in Fig. 12) of the FC magnetic hysteresis loops measured along the [001] axis in the temperature range between 3 K and 200 K. The inset image in Fig. 11 shows parts of the ZFC loops with typical double shifted symmetrical shape, which disappears around 50 K. Similar to the FC loops in Fig. 5 the loops in Fig. 11 recorded along the easy direction shift from the origin indicating the EB effect but at the same time they magnetize more easily and show almost twice as high remnant magnetization as the loops recorded for the SA sample. The coercivity is distinctly reduced as is well visible from the inset in Fig. 12. The inset figure shows the H_E and H_C dependencies on temperature for the SA and SV specimens. It is seen

that the application of the magnetic field along the easy direction of uniaxial SV has little effect on EB as compared to the SA sample but coercivity decreases. In both cases EB disappears around 100 K, which is typically observed for these systems [19]. In order to determine the value of uniaxial magnetic anisotropy constant K_u as a function of temperature isothermal *M* vs. *H* curves were recorded between 2 and 250 K. The upper temperature limit was set by the proximity to the temperature of the reverse transformation, which was maintained at the distance of circa 50 K in view of the applied magnetic field intensity of up to 7 T. The values of K_u were calculated at each temperature from the *M* vs. *H* curves as the area between the easy *c* axis and the hard *a* axis [37]. The results are shown in Fig. 13 (d). K_u saturates at low temperatures at the level of 7×10^4 J/m^3 and then continuously decreases with increasing temperature as the system approaches the Curie temperature of martensite. The value of the anisotropy constant is generally considerably lower than the equivalent values in Ni-Mn-Ga system [38,39]. For comparison with ferromagnetic MSMA, which are capable of MFIS associated with twin boundary motion, K_u in order to yield MFIS in such systems should be larger than the product of ϵ_0 and the twinning stress σ_{tw}, what can be written as: $K_u \geq \epsilon_0 \times \sigma_{tw}$. On average σ_{tw} is found around 2 MPa in Ni-Mn-Ga [36,37]. In the present case σ_{tw} as calculated from the determined K_u at 3 K and theoretical maximal strain K_u/ϵ_0 should be at the level of or less than 8.5 MPa. From the stress strain curve in Fig. 6 denoted as number 4 and corresponding to the fourth compression test, for which it is allowed for assuming that at the start of the test the system rests in the single variant state, the σ_{tw} as estimated from the knee on the curve just after the elastic range is around 18.8 MPa. It therefore becomes evident that even at low temperature below the Curie temperature of martensite MFIS due twin boundary motion in the studied Ni-Mn-Sn single crystal is not feasible since K_u is too low. The low value of the magnetic anisotropy constant near the temperature of the reverse MT confirms further quantitatively that the magnetic anisotropy energy has a negligible contribution to the magnetic field induced reverse martensitic transformation in the studied Ni-Mn-Sn single crystal. Based on the definition of the magneto crystalline anisotropy energy, which accounts for the magnetization difference between the hard and easy axes of the ferromagnetic single martensite variant [5], it could be expected that the application of the magnetic field along the easy axis of the pre-trained single martensite variant would reduce the critical magnetic field, or in other words, the critical stress necessary to initiate the reverse MT, provided that K_u was considerable. This could be deduced from the formula combining the factors contributing to the minimization of the magnetic energy: $F = \pm K_u m_x^2 + M^2(m \cdot D \cdot m) - mHM$, where K_u is the uniaxial anisotropy constant, m is the magnetic moment, D is a demagnetization tensor and the ± sign corresponds to positive or negative K_u with respect to the orientation of the easy magnetization axes of a given variant to the applied magnetic field [40]. It henceforth becomes clear that due to the low value of K_u in the system studied it is the Zeeman energy arising in the magnetization difference between the martensite and austenite phases, which is chiefly responsible for the metamagnetic behaviour in the $Ni_{50}Mn_{37.5}Sn_{12.5}$ single crystal, regardless of its orientation in single variant martensite state along the applied magnetic field.

IV. Conclusions

The structural and magnetic properties of $Ni_{50}Mn_{37.5}Sn_{12.5}$ single crystal were investigated. The alloy undergoes martensitic transformation at 308 K from the austenite phase to the structurally modulated tetragonal 4M martensite phase with lattice parameters

a_{4M} = 6.177 Å, c_{4M} = 5.669 Å and $(3\bar{1})$ shuffling modulation period according to Zhdanov notation. The alloy shows 7.9% pre-strain upon uniaxial compression test performed along the <001> direction, which is near the theoretical 8.2% maximum twinning strain calculated as $\epsilon_0 = (1 - c/a)$. Magnetization measurements reveal that the magnetic anisotropy of the martensite phase is uniaxial with easy magnetization axis corresponding to the shortest *c* - axis of the tetragonal distortion, while *a* - axis is hard magnetization direction. The magnetic anisotropy constant K_u determined at 3 K is equal to 7×10^4 J/m^3 and then gradually decreases with increasing temperature as the system approaches the Curie temperature of martensite, which occurs at 215 K.

Acknowledgments

The financial support of the Polish National Science Centre (NCN) – Project number: 2012/07/N/ST8/03918 is gratefully acknowledged.

References

[1] R. Kainuma, Y. Imano, W. Ito, Y. Sutou, H. Morito, S. Okamoto, O. Kitakami, K. Oikawa, A. Fujita, T. Kanomata, K. Ishida, Magnetic-field-induced shape recovery by reverse phase transformation, Nat. Lett. 439 (2006) 957-960.
[2] X. Moya, Ll. Manosa, A. Planes, T. Krenke, M. Acet, E. F. Wassermann, Martensitic transition and magnetic properties in Ni-Mn-X alloys, Mater. Sci. Eng. A 438-440 (2006) 911-915.
[3] M. Acet, E. F. Wassermann, Magnetic interactions in Ni-Mn-based magnetic shape-memory Heusler alloys, Adv. Eng. Mater. 14 (2012) 523-529.
[4] K. Koyama, K. Watanabe, T. Kanomata, R. Kainuma, K. Oikawa, K. Ishida, Observation of field-induced reverse transformation in ferromagnetic shape memory alloy $Ni_{50}Mn_{36}Sn_{14}$, Appl. Phys. Lett. 88 (2006) 132505-1-3.
[5] H. E. Karaca, I. Karaman, B. Basaran, Y. Ren, Y. I. Chumlyakov, H. J. Maier, Magnetic Field-Induced Phase Transformation in NiMnCoIn Magnetic Shape-Memory Alloys – A New Actuation Mechanism with Large Work Output, Adv. Funct. Mater. 19 (2009) 983-998.
[6] W. Ito, X. Xu, R. Y. Umetsu, T. Kanomata, K. Ishida, R. Kainuma, Concentration dependence of magnetic moment in $Ni_{50-x}Co_xMn_{50-y}Z_y$ (Z=In, Sn) Heusler alloys, Appl. Phys. Lett. 97 (2010) 242512-1-3.
[7] H. E. Karaca, I. Karaman, B. Basaran, Y. I. Chumlyakov, H. J. Maier, Magnetic field and stress induced martensite reorientation in NiMnGa ferromagnetic shape memory alloy single crystals, Acta Mater. 54 (2006) 233-245.
[8] A. Sozinov, N. Lanska, A. Soroka, W. Zou, 12% magnetic field-induced strain in Ni-Mn-Ga-based non-modulated martensite, Appl. Phys. Lett. 102 (2013) 021902.
[9] J. Enkovaara, A. Ayuela, A. T. Zayak, P. Entel, L. Nordstrom, M. Dube, J. Jalkanen, J. Impola, R. M. Nieminen, Magnetically driven shape memory alloys, Mater. Sci. Eng. A 378 (2004) 52-60.
[10] H. E. Karaca, I. Karaman, B. Basaran, D. C. Lagoudas, Y. I. Chumlyakov, H. J. Maier, On the stress-assisted magnetic-field-induced phase transformation in Ni_2MnGa ferromagnetic shape memory alloys, Acta Mater. 55 (2007) 4253-4269.
[11] A. Vassiliev, Magnetically driven shape memory alloys, J. Magn. Magn. Mater. 242-245 (2002) 66-67.
[12] H. E. Karaca, I. Karaman, A. Brewer, B. Basaran, Y. I. Chumlyakov, H. J. Maier, Shape memory and pseudoelasticity response of NiMnCoIn magnetic shape memory alloy single crystals, Scripta Mater. 58 (2008) 815-818.
[13] J. A. Monroe, I. Karaman, B. Basaran, W. Ito, R. Y. Umetsu, R. Kainuma, K. Koyama, Y. I. Chumlyakov, Direct measurement of large reversible magnetic-field-induced strain in Ni-Co-Mn-In metamagnetic shape memory alloys, Acta Mater. 60 (2012) 6883-6891.
[14] N. M. Bruno, I. Karaman, J. H. Ross Jr., Y. I. Chumlyakov, High-field magneto-thermo-mechanical testing system for characterizing multiferroic bulk alloys, Rev. Sci. Instrum. 86 (2015) 113902-1-11.
[15] R. Kainuma, Y. Imano, W. Ito, H. Morito, Y. Sutou, K. Oikawa, A. Fujita, K. Ishida, S. Okamoto, O. Kitakami, T. Kanomata, Metamagnetic shape memory effect in a Heusler-type $Ni_{43}Co_7Mn_{39}Sn_{11}$ polycrystalline alloy, Appl. Phys. Lett. 88 (2006) 192513-1-3.
[16] V. Sanchez-Alarcos, V. Recarte, J. I. Perez-Landazabal, E. Cesari, J. A. Rodriguez-Velamazan, Long-Range Atomic Order and Entropy Change at the Martensitic Transformation in a Ni-Mn-In-Co Metamagnetic Shape Memory Alloy, Entropy 16 (2014) 2756-2767.

[17] N. M. Bruno, C. Yegin, I. Karaman, J-H. Chen, J. H. Ross Jr., J. Liu, J. Li, The effect of heat treatments on $Ni_{43}Mn_{42}Co_4Sn_{11}$ meta-magnetic shape memory alloys for magnetic refrigeration, Acta Mater. 74 (2014) 66-84.
[18] M. Khan, A. K. Pathak, M. R. Paudel, I. Dubenko, S. Stadler, N. Ali, Magnetoresistance and field-induced structural transitions in $Ni_{50}Mn_{50-x}Sn_x$ Heusler alloys, J. Magn. Magn. Mater. 320 (2008) L21-L25.
[19] M. Khan, I. Dubenko, S. Stadler, N. Ali, Exchange bias in bulk Ni-Mn-Sn Heusler alloys, J. Appl. Phys. 102 (2007) 113914-1-4.
[20] A. Planes, Ll. Mnosa, X. Moya, T. Krenke, M. Acet, E. F. Wassermann, Magnetocaloric effect in Heusler shape-memory alloys, J. Magn. Magn. Mater. 310 (2007) 2767-2769.
[21] S. Fahler, U. K. Rossler, O. Kastner, J. Eckert, G. Eggeler, H. Emmerich, P. Entel, S. Muller, E. Quandt, K. Albe, Caloric Effects in Ferroic Materials: New Concepts for Cooling, Adv. Eng. Mater. 14 (2012) 10-19.
[22] W. Sun, J. Liu, B. Lu, Y. Li, A. Yan, Large elastocaloric effect at small transformation strain in $Ni_{45}Mn_{44}Sn_{11}$ metamagnetic shape memory alloys, Scripta Mater. 114 (2016) 1-4.
[23] Y. Sutou, Y. Imano, N. Koeda, T. Omori, R. Kainuma, K. Ishida, K. Oikawa, Magnetic and martensitic transformations of NiMnX(X=In, Sn, Sb) ferromagnetic shape memory alloys, Appl. Phys. Lett. 85 (2004) 4358-4360.
[24] J. D. Garrett, J. E. Greedan, K. E. Locke, C. V. Stager, Growth of large single crystals of Heusler alloys, $Ni_2Mn_{1-x}V_xSn$, for neutron inelastic scattering experiments, J. Cryst. Growth 46 (1979) 463-466.
[25] M. J. Szczerba, R. Chulist, Detwinning of a non-modulated Ni-Mn-Ga martensite: From self-accommodated microstructure to single crystal, Acta Mater. 85 (2015) 67-73.
[26] P. Czaja, M. Fitta, J. Przewoźnik, W. Maziarz, J. Morgiel, T. Czeppe, E. Cesari, Effect of heat treatment on magnetostructural transformations and exchange bias in Heusler $Ni_{48}Mn_{39.5}Sn_{9.5}Al_3$ ribbons, Acta Mater. 103 (2016) 30-45.
[27] T. Krenke, M. Acet, E. F. Wassermann, X. Moya, Ll. Manosa, A. Planes, Martensitic transitions and the nature of ferromagnetism in the austenitic and martensitic states of Ni-Mn-Sn alloys, Phys. Rev. B 72 (2005) 014412-1-9.
[28] P. J. Shamberger, F. S. Ohuchi, Hysteresis of the martensitic phase transition in magnetocaloric-effect Ni-Mn-Sn alloys, Phys. Rev. B 79 (2009) 144407-1-9.
[29] I. Titov, M. Acet, M. Farle, D. Gonzalez-Alonso, L. Manosa, A. Planes, T. Krenke, Hysteresis effects in the inverse magnetocaloric effect in martensitic Ni-Mn-In and Ni-Mn-Sn, J. Appl. Phys. 112 (2012) 073914-1-5.
[30] P. Czaja, R. Chulist, M. J. Szczerba, J. Przewoźnik, E. Olejnik, A. Chrobak, W. Maziarz, E. Cesari, Magnetostructural transition and magnetocaloric effect in highly textured Ni-Mn-Sn alloy, J. Appl. Phys. 119 (2016) 165102-1-6.
[31] R. Kainuma, Y. Imano, W. Ito, H. Morito, Y. Sutou, K. Oikawa, A. Fujita. K. Ishida, S. Okamoto, O. Kitakami, T. Kanomata, Metamagnetic shape memory effect in a Heusler-type $Ni_{43}Co_7Mn_{39}Sn_{11}$ polycrystalline alloy, Appl. Phys. Lett. 88 (2006) 192513-1-3.
[32] M. Pasquale, C. P. Sasso, L. H. Lewis, L. Giudici, T. Lograsso, D. Schlagel, Magnetostructural transition and magnetocaloric effect in $Ni_{55}Mn_{20}Ga_{25}$ single crystal, Phys. Rev. B 72 (2005) 094435-1-5.
[33] M. J. Szczerba, R. Chulist, S. Kopacz, M. S. Szczerba, Effect of initial plastic prestrain on mechanical training of non-modulated Ni-Mn-Ga martensite structure, Mater. Sci. Eng A 611 (2014) 313-319.
[34] M. J. Szczerba, „Struktura i właściwości monokryształów magnetycznych stopów Ni-Mn-Ga", PhD thesis, Institute of Metallurgy and Materials Science Polish Academy of Sciences, Kraków 2010.
[35] R. Chulist, "Structure and Properties of Twin Boundaries in Ni-Mn-Ga Alloys", PhD thesis, Technische Universitat Dresden, Dresden 2011.
[36] A. Sozinov, A. A. Likhachev, N. Lanska, O. Soderberg, K. Ullakko, V. K. Lindroos, Stress- and magnetic-field-induced variant rearrangement in Ni-Mn-Ga single crystals with seven-layered martensitic structure, Mater. Sci. Eng. A378 (2004) 399-402.
[37] A. Sozinov, A. A. Likhachev, N. Lanska, K. Ullakko, Giant magnetic-field-induced strain in Ni-Mn-Ga seven-layered martensitic phase, Appl. Phys. Lett. 80 (2002) 1746-1748.
[38] O. Heczko, L. Straka, N. Lanska, K. Ullakko, J. Enkovaara, Temperature dependence of magnetic anisotropy in Ni-Mn-Ga alloys exhibiting giant field-induced strain, J. Appl. Phys. 91 (2002) 8228-8230.
[39] L. Straka, O. Heczko, K. Ullakko, Investigation of magnetic anisotropy of Ni-Mn-Ga seven-layered orthorombic martensite, J. Magn. Magn. Mater. 272-276 (2004) 2049-2050.
[40] C. P. Sasso, V. A. L'vov, V. A. Chernenko, J. M. Barandiaran, M. Pasquale, Reorientation of Ni-Mn-Ga martensite in rotating magnetic field, Physics Procedia 10 (2010) 149-153.

List of figures:

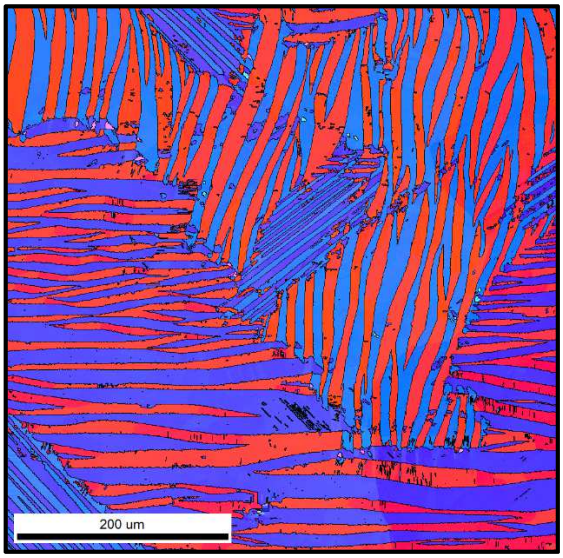

Fig. 1. EBSD map of the self-accommodated 4M martensite microstructure.

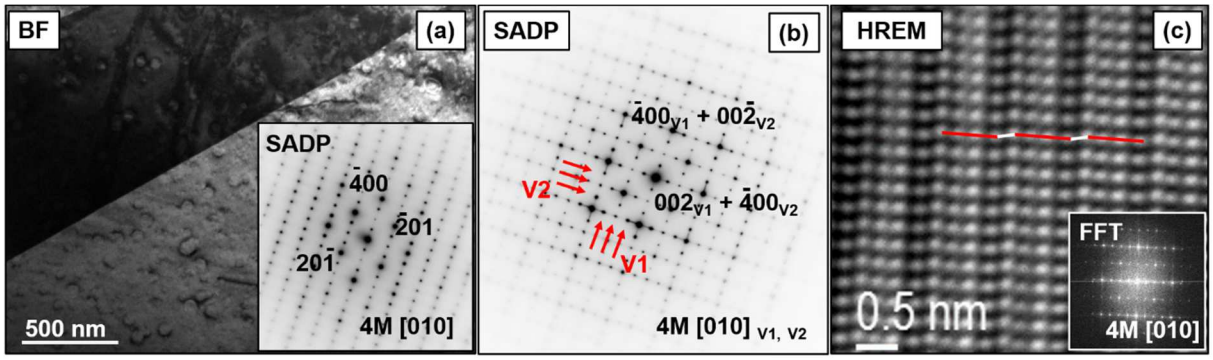

Fig. 2. TEM BF image and corresponding SADP (inset) for a single variant (a), SADP for two twinned variants V1 + V2 with nearly orthogonal modulation direction (b), HREM image and corresponding FFT (inset) from a single variant (c).

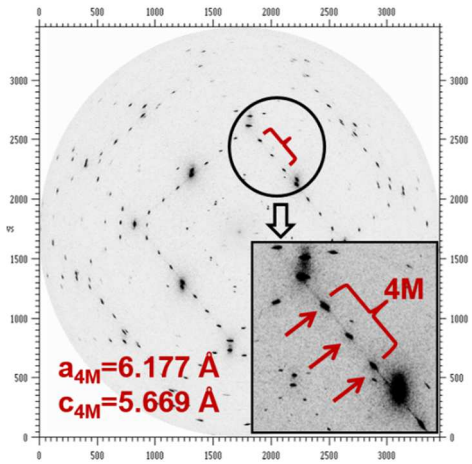

Fig. 3. Synchrotron high energy X-ray diffraction pattern of the $Ni_{49.5}Mn_{38.4}Sn_{12.2}$ sample at RT.

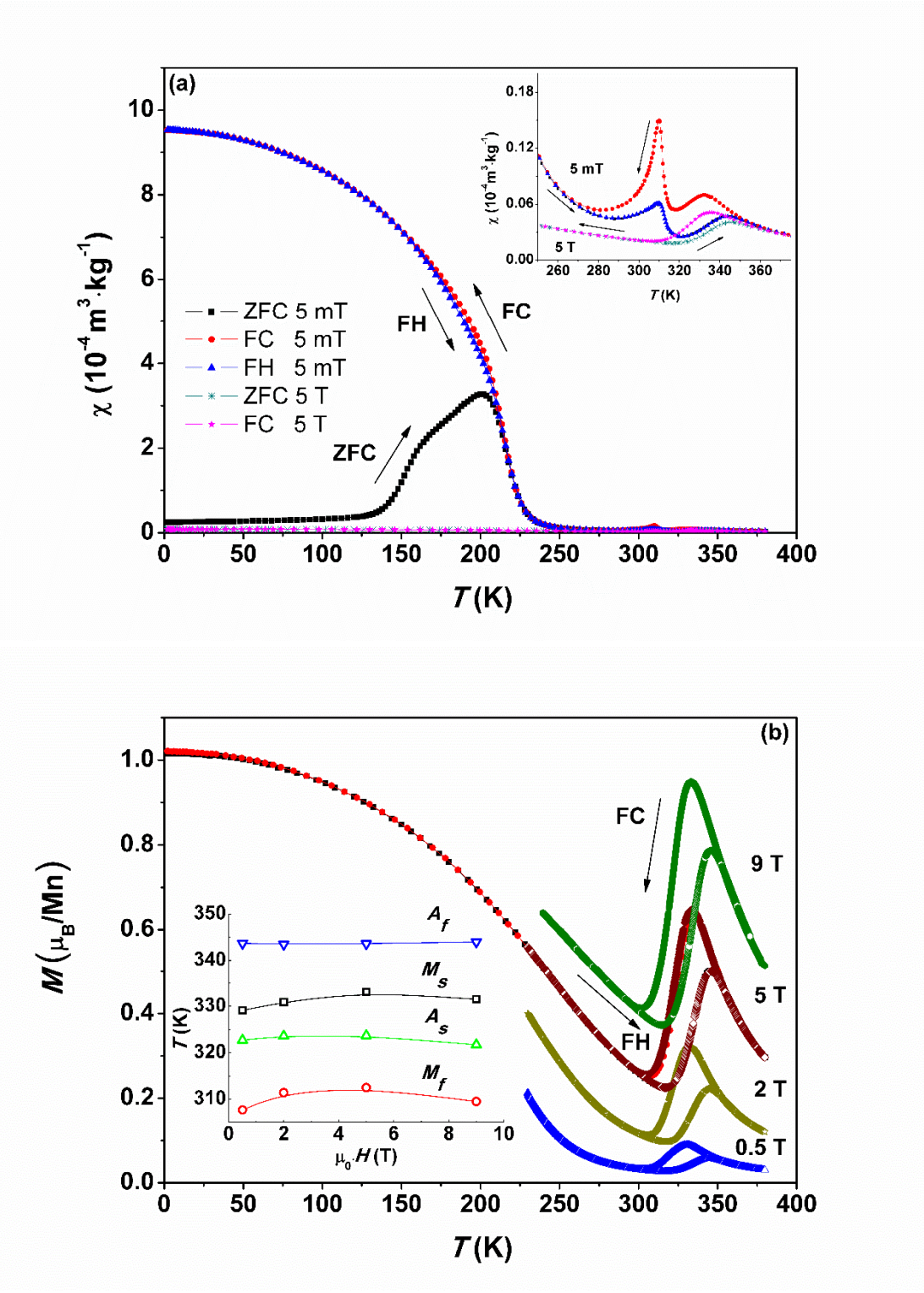

Fig. 4. Thermomagnetization curves of the SA $Ni_{49.5}Mn_{38.4}Sn_{12.2}$ single crystal under magnetic fields of 5 mT and 5 T (a), and under 0.5 up to 9 T (b). The inset figure shows forward M_s, M_f and reverse A_s, A_f martensitic transformation temperatures, as determined from the thermomagnetization curves, vs. magnetic field intensity.

Inset in Fig. 4 (b) has been updated.

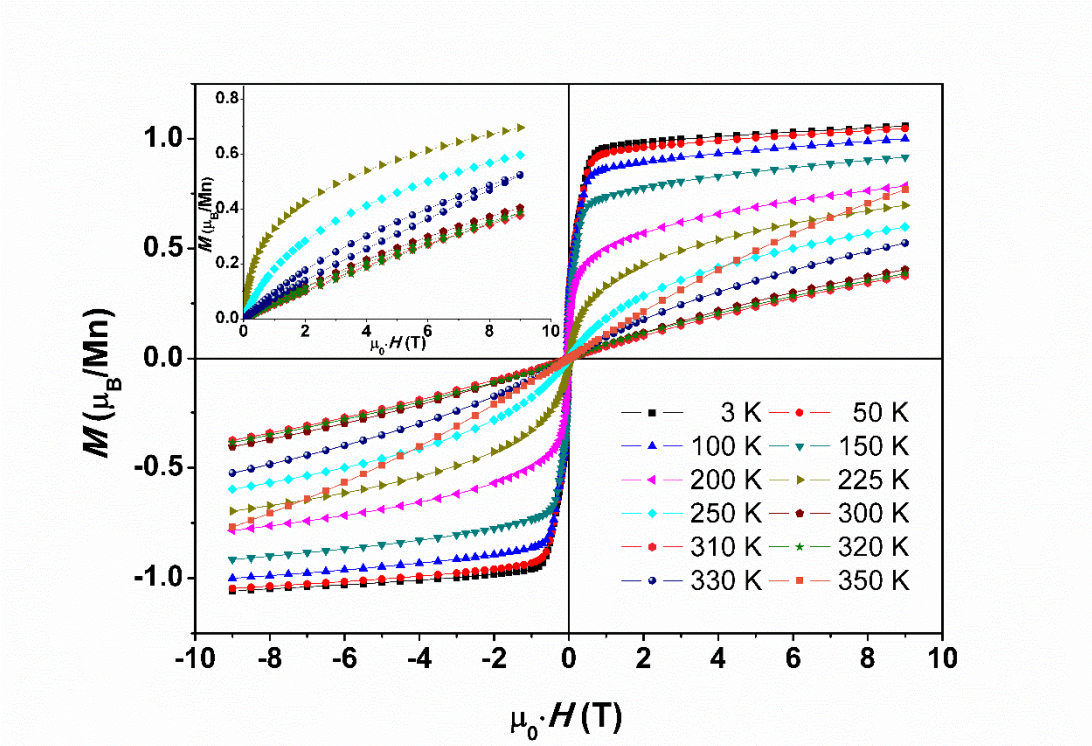

Fig. 5. Field dependence of FC magnetization (M) isotherms for SA $Ni_{49.5}Mn_{38.4}Sn_{12.2}$ single crystal at the temperature range of 3-350 K. The inset shows the halves of selected M vs. H curves near the temperature of the reverse martensitic transformation.

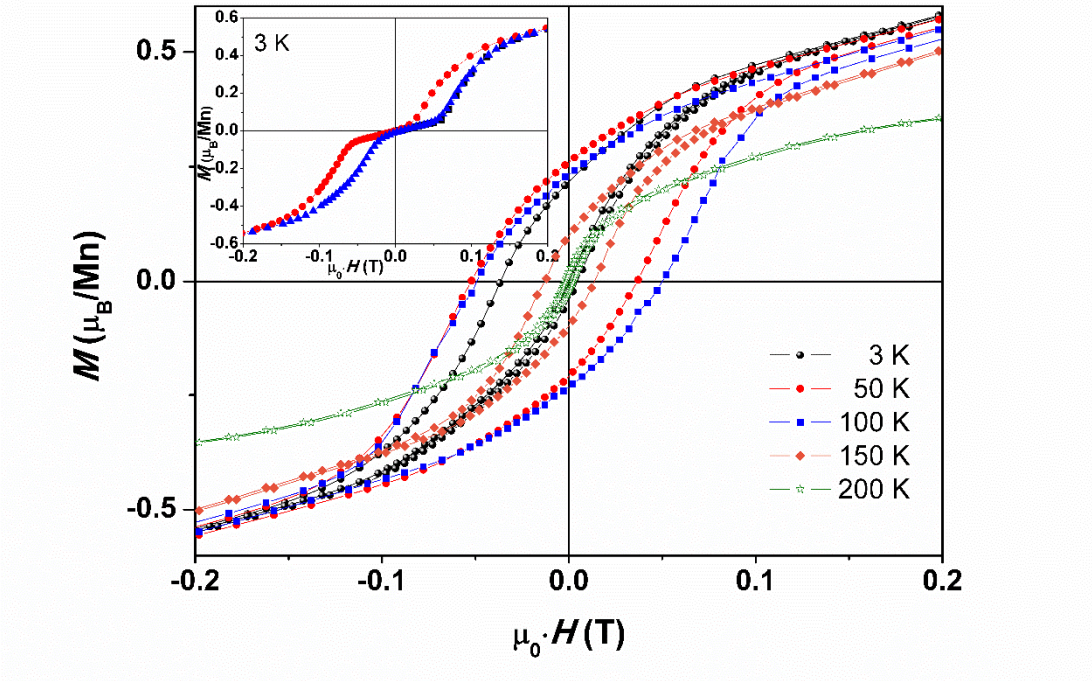

Fig. 6. Parts of the FC hysteresis loops of SA $Ni_{49.5}Mn_{38.4}Sn_{12.2}$ single crystal measured at the temperature range between 3 and 200 K; the inset picture shows ZFC hysteresis loops measured for the same sample at 3 K.

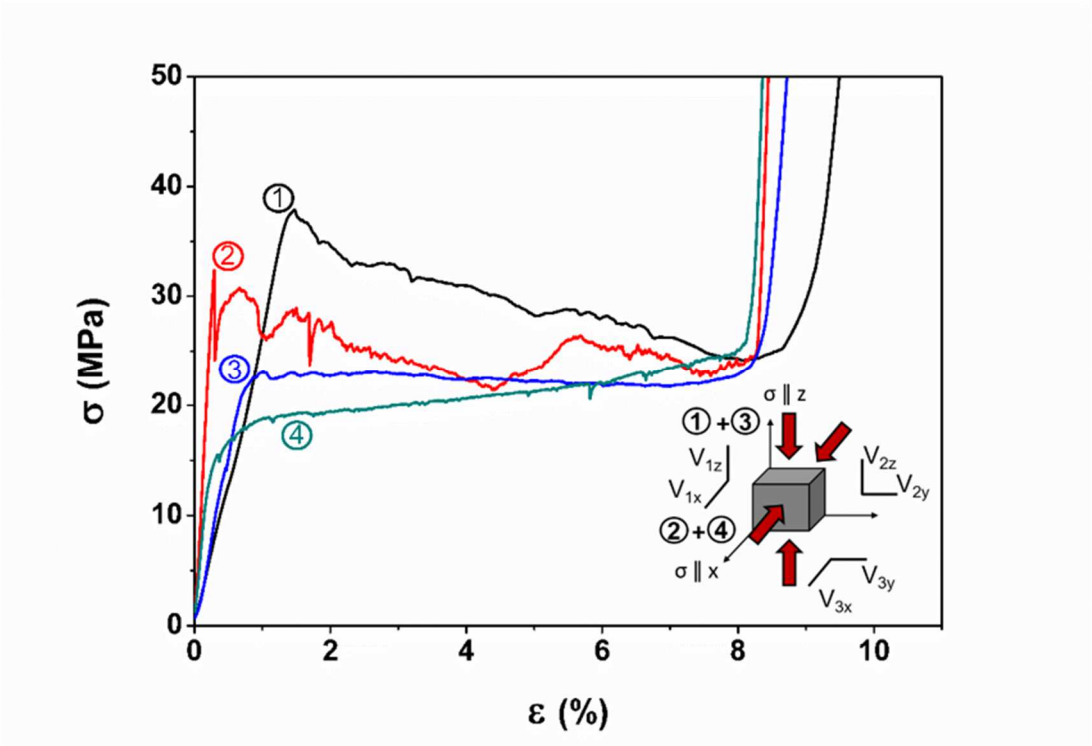

Fig. 7. Stress (σ) vs. strain (ε) curves for martensitic reorientation. The σ (ε) curves were recorded at room temperature for compressions of the initially martensitic self-accommodated multivariant structure. The sample layout is shown in the inset along with the schematics of the compression sequence.

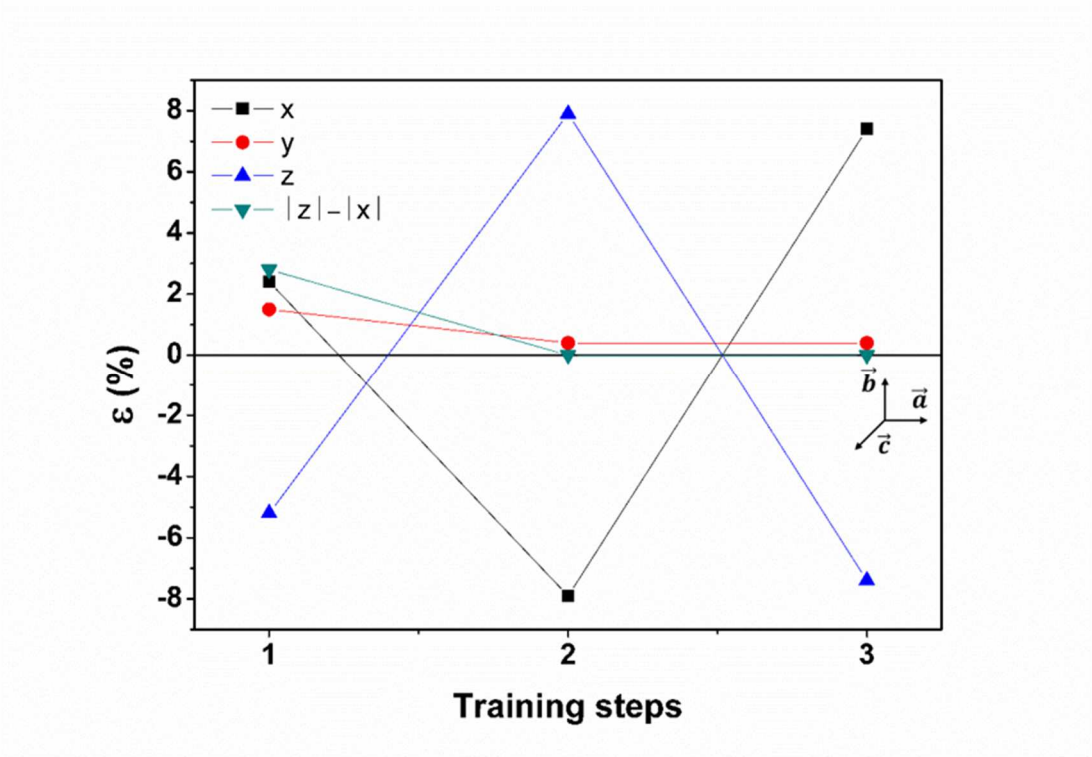

Fig. 8. Strain along *x*, *y* and *z* axes accompanying each of the four mechanical training steps. The solid line is a guide for eyes. The inset schematic shows the $\vec{a}$, $\vec{b}$, $\vec{c}$ crystal lattice vectors relative to *x*, *y* and *z* axes after the fourth compression test.

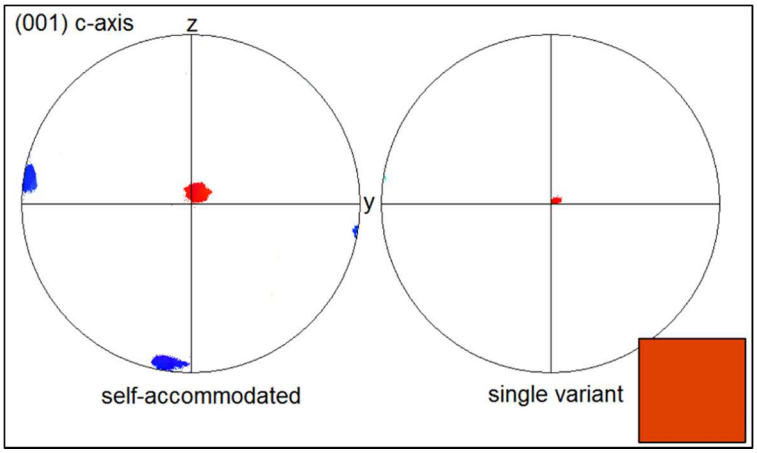

Fig. 9. Pole figure (001) representing c-axis before and after the training procedure; the inset picture shows the EBSD map taken after the training from the same sample area as shown in Fig. 1 prior to mechanical testing.

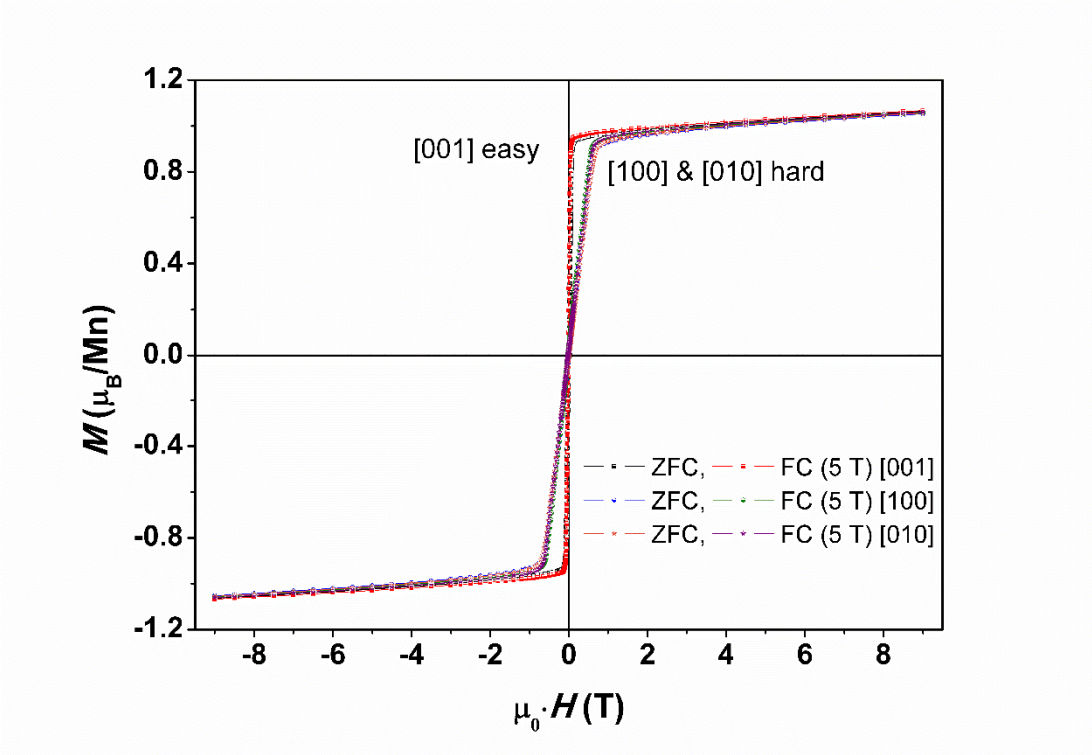

Fig. 10. Magnetization curves measured along [100] ($\vec{a}$), [010] ($\vec{b}$) and [001] ($\vec{c}$) directions of the single variant 4 M martensite in the $Ni_{49.5}Mn_{38.4}Sn_{12.2}$ at 3 K.

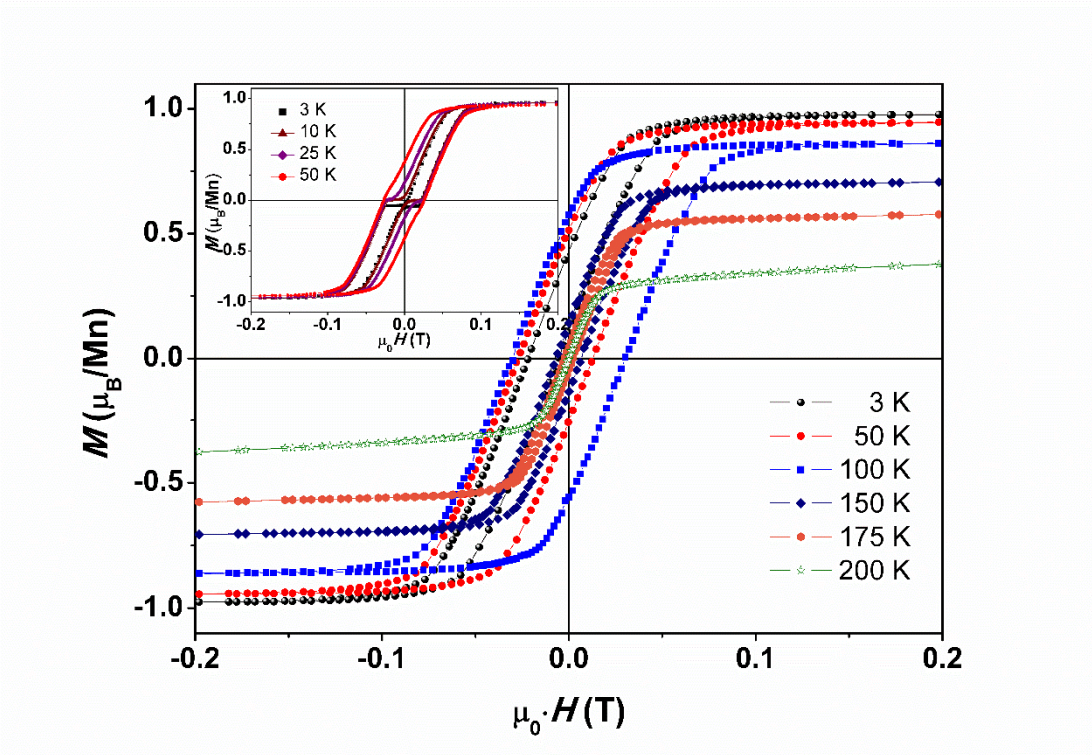

Fig. 11. Parts of the FC hysteresis loops of the SV $Ni_{49.5}Mn_{38.4}Sn_{12.2}$ measured along [001] ($\vec{c}$) direction at the temperature range between 3 and 200 K; the inset picture shows ZFC hysteresis loops measured for the same sample at 3 K, 10 K, 25 K and 50 K.

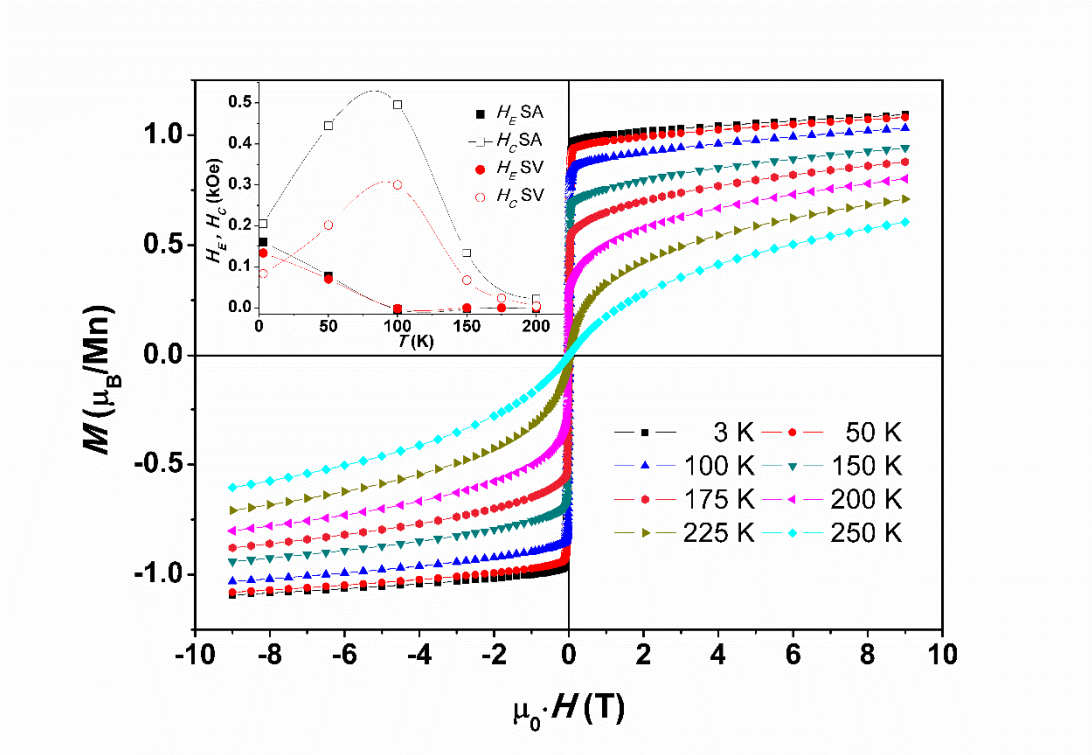

Fig. 12. Field dependence of FC magnetization (*M*) isotherms measured along [001] ($\vec{c}$) direction for SV $Ni_{49.5}Mn_{38.4}Sn_{12.2}$ at the temperature range of 3-250 K; the inset: H_E and H_C vs. temperature dependencies for SA and SV $Ni_{49.5}Mn_{38.4}Sn_{12.2}$ single crystal measured at the temperature range between 3 and 200 K after FC at 5 T.

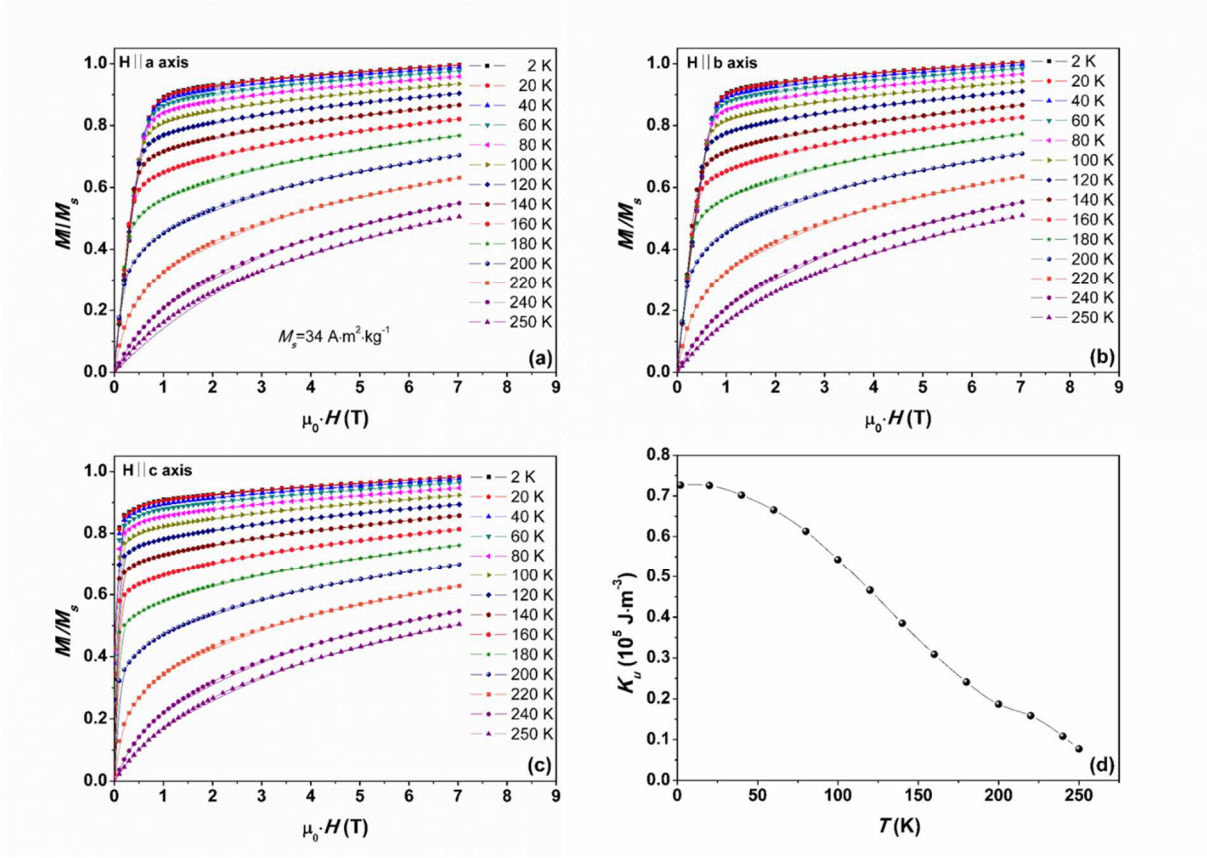

Fig. 13. Magnetization vs. magnetic field isotherms measured along [100] ($\vec{a}$), [010] ($\vec{b}$) hard axes and [001] ($\vec{c}$) easy axis of the SV $Ni_{49.5}Mn_{38.4}Sn_{12.2}$ single crystal at the temperature range between 2 and 250 K, (a), (b), (c); Magnetic anisotropy constant K_u of the single variant 4 M martensite as a function of temperature (d).

Table 1. The characteristic M_s, M_f, A_s, and A_f temperatures determined from the respective FC and FH curves at higher magnetic field along with the values of transformation hysteresis given as A_f - M_s or A_s - M_f and transformation interval calculated as M_s - M_f and A_f - A_s.

(T)	**(K)**							
$\mu_0 \cdot H$	M_s	M_f	A_s	A_f	A_f - M_s	A_s - M_f	M_s - M_f	A_f - A_s
0.5	329	308	323	344	15	15	21	21
2	331	311	324	343	12	13	20	19
5	333	313	324	344	11	11	20	20
9	332	310	322	344	12	12	22	22